On the long-time behavior of the continuous and discrete solutions of a nonlocal Cahn–Hilliard type inpainting model

Dandan Jiang, Mejdi Azaiez, Alain Miranville, Chuanju Xu, Hui Yao

ON THE LONG-TIME BEHAVIOR OF THE CONTINUOUS AND DISCRETE SOLUTIONS OF A NONLOCAL CAHN-HILLIARD TYPE INPAINTING MODEL

DANDAN JIANG[1], MEJDI AZAIEZ[2], ALAIN MIRANVILLE[3], CHUANJU XU[1,†], HUI YAO[2]

Abstract. In this paper, we study the analytical and numerical long-time stability of a nonlocal Cahn-Hilliard model with a fidelity term for image inpainting introduced in our previous work [1]. First, we establish the uniform boundedness of the continuous problem in both L^2 and H^1 spaces, which is obtained by using the Gagliardo-Nirenberg inequality and the uniform Grönwall lemma. Then, for the temporal semi-discrete scheme, the uniform estimates in L^2 and H^1 spaces are derived with the aid of the discrete uniform Grönwall lemma under a suitable assumption on the nonlinear potential. This demonstrates the long-time stability of the proposed scheme in L^2 and H^1 spaces. Finally, we validate the long-time stability and the applicability of our method in signal reconstruction and image inpainting. These numerical experiments demonstrate the high effectiveness of our proposed model.

1. Introduction

There have been a large body of literatures on image inpainting/denoising models, see, e.g., [2–11] and their references. The classical Cahn-Hilliard equation was initially proposed as a phenomenological model to describe the process of spinodal decomposition (or phase separation) in binary alloys by Cahn and Hilliard [12], and it has become a fundamental framework used in many fields ranging from physics, materials science to finance, as well as image processing. In image inpainting, Bertozzi et al. [13, 14] originally proposed and analysed a Cahn-Hilliard type inpainting model with fidelity term for binary images. Subsequently, a large number of generalized Cahn-Hilliard type models have been developed for image processing; see, e.g., [10, 15–18] and references therein. However it has been well-known that a drawback of this kind of models is the over-smoothing effect of the edges that overlap with the inpainting region, see, e.g., [10, 14, 19].

In recent years, the nonlocal and space-fractional Cahn-Hilliard models have been applied in materials science and image science. Compared with the classical Cahn-Hilliard model, nonlocal models have more advantages in modeling anomalous diffusion and long-range interactions. Many works have been dedicated to the development of numerical methods for the nonlocal Cahn-Hilliard model (see [20–29]). In particular, [20–22] designed and analyzed the numerical schemes for the periodic nonlocal Cahn-Hilliard model. [26, 27] revealed that the nonlocal Cahn-Hilliard model analytically and computationally supports discontinuous steady-state solutions, and exhibits sharper

Key words and phrases. Image inpainting, nonlocal Cahn-Hilliard model, long-time stability, uniform estimates.
*This research is partially supported by NSFC grant 12371408 and ANR-22-CE46-0005 NumOpTES.
[1]School of Mathematical Sciences and Fujian Provincial Key Laboratory of Mathematical Modeling and High Performance Scientific Computing, Xiamen University, 361005 Xiamen, China.
[2]University of Bordeaux, Laboratoire I2M UMR 5295, 33400 Talence, France.
[3]Laboratoire de Mathématiques et Applications, Université de Poitiers, Site du Futuroscope - Téléport 2, 11 Boulevard Marie et Pierre Curie - Bâtiment H3 - TSA 61125, 86073 Poitiers, France.
[†]Corresponding author.
Emails: dandanjiang@stu.xmu.edu.cn (D. Jiang); azaiez@u-bordeaux.fr (M. Azaiez); alain.miranville@math.univ-poitiers.fr (A. Miranville); cjxu@xmu.edu.cn (C. Xu); hui.yao@u-bordeaux.fr (H. Yao).

interfaces under suitable model parameters than the local Cahn-Hilliard model. In addition, researchers have explored the fractional Cahn-Hilliard equations with different fractional operators defined in [30–32] for image inpainting (see [33–36] and reference therein). Our recent work [1] proposed and analyzed a nonlocal Cahn-Hilliard type model for image inpainting and an efficient numerical scheme was constructed based on the convexity splitting method.

We briefly recall the nonlocal Cahn-Hilliard type inpainting model introducuded in [1]. Let $\Omega \in \mathbb{R}^d$ $(d = 1, 2)$ be a bounded rectangular domain, $D \subset \Omega$ be the inpainting region. The final time $T > 0$ is arbitrarily fixed. Given a damaged image $f \in L^2$, the evolution of the inpainted image u is governed by the following equations:

$$\frac{\partial u}{\partial t} = \Delta \mu + \lambda (f - u), \quad \text{in} \quad \Omega \times [0, T], \tag{1.1a}$$

$$\mu = \varepsilon \mathcal{L}(u) + \frac{1}{\varepsilon} W'(u), \quad \text{in} \quad \Omega \times [0, T], \tag{1.1b}$$

subject to suitable boundary condition. λ is the fidelity parameter given by:

$$\lambda = \begin{cases} \lambda_0, & \text{in } \Omega \setminus D, \\ 0, & \text{in } D, \end{cases}$$

where $\lambda_0 > 0$ is a large enough constant. $\lambda (f - u)$ is the fidelity term, forcing the inpainted image u (the stationary solution of (1.1)) be aligned with f in undamaged domain $\Omega \setminus D$. $\varepsilon > 0$ is the diffused interface thickeness. $\mathcal{L} : \mathrm{L}^2_{\mathrm{per}}(\Omega) \to \mathrm{L}^2_{\mathrm{per}}(\Omega)$ is the nonlocal operator introduced in [21, 37], which is self-adjoint, positive semi-definite and mean-zero, defined by

$$\mathcal{L} : v(\boldsymbol{x}) \mapsto \int_\Omega J(\boldsymbol{x} - \boldsymbol{y})(v(\boldsymbol{x}) - v(\boldsymbol{y}))\mathrm{d}\boldsymbol{y}, \tag{1.2}$$

where $J \geq 0$ is a radial function with positive integral. $W(u) = u^2(1 - u)^2$.

Equation (1.1) is associated to the total energy:

$$E = \underbrace{\frac{\varepsilon}{2}(\mathcal{L}u, u) + \int_\Omega \frac{1}{\varepsilon} W(u)\mathrm{d}\boldsymbol{x}}_{E_1} + \underbrace{\frac{\lambda}{2}\int_\Omega (f - u)^2 \mathrm{d}\boldsymbol{x}}_{E_2}. \tag{1.3}$$

In fact, the first term on the right hand of (1.1a) is the gradient of E_1 in H^{-1} space [38], and the second term is the gradient of E_2 in L^2. This indicates that rather than being a gradient flow of (1.3) in a specific space, (1.1) is a superposition of the H^{-1} gradient flow of E_1 and the L^2 gradient flow of E_2. The existence and uniqueness of the weak solution of (1.1) have been established in [39], while the well-posedness of the stationary solution of (1.1) is given in [1].

Most related work have focused on the energy stability and convergence analysis of numerical methods for nonlocal or space-fractional Cahn-Hilliard models. Several works have been done on the long time dynamical properties of continuous dynamical systems (see [40–48] and reference therein). Some studies have explored the long-time behavior of numerical schemes for some nonlinear evolutional equations, like the Navier-Stokes equations [49–54], magneto-hydrodynamics equations [55], Cahn-Hilliard and Allen-Cahn equations [56–60], and etc. However, due to the difficulties arising from the long-range interactions of the nonlocal operator $\mathcal{L}$ defined in (1.2), there are few works on the long-time stability property of numerical methods for nonlocal models in the existing literature.

The main purpose of this paper is to investigate the long-time dynamics for the continuous problem (1.1) and its discretization proposed in our recent work [1]. We first prove the long-time stability of the continuous problem (1.1) in L^2 and H^1 norms. Then we show that the time semi-discrete scheme, based on the convexity splitting method, preserves the long-time stability of

(1.1). To the best of our knowledge, this is the first work investigating the numerical long-time stability of the nonlocal Cahn-Hilliard equation with fidelity term, especially for image inpainting. In practice, these theoretical results provide strong guidance in application, guaranteeing that the final state of the image does not depend on the initial data under suitable conditions.

The rest of the paper is organized as follows. In the next section, we give some notations, assumptions, and properties of the kernel J, as well as provide some preliminary inequalities and lemmas used in our analysis. In Section 3, we consider the long-time stability of the continuous problem (1.1) in L^2 and H^1 norms. In Section 4, we first present the time discretization of (1.1), then provide a rigorous analysis that develops conditions sufficient to guarantee long-time stability in both L^2 and H^1 norms. In Section 5, we confirm the theoretical results and show the efficiency of the proposed model on signal reconstruction and image inpainting. Finally, a brief summary is given in Section 6.

2. Preliminaries

We begin with giving some notations and recall some preliminary facts on the nonlocal operator. Throughout this paper, we assume that the kernel $J \in W^{1,1}(\Omega)$ always satisfies the following conditions:
(a) $J(\boldsymbol{x}) \geq 0$ for any $\boldsymbol{x} \in \Omega$,
(b) J is a radial function and has finite support, i.e. $J(\boldsymbol{x}) = j(|\boldsymbol{x}|)$ for a single-variable function j with $\mathrm{supp}(j) \subset (0, \kappa]$, $\kappa > 0$, and there exists $\kappa_1 > 0$, such that $(0, \kappa_1) \subset \mathrm{supp}(j)$,
(c) J is Ω-periodic,
(d) $\frac{1}{2}\int_\Omega J(\boldsymbol{x})|\boldsymbol{x}|^2 \,\mathrm{d}\boldsymbol{x} = 1$,
(e) $0 \leq a := a(\boldsymbol{x}) = \int_\Omega J(\boldsymbol{x}-\boldsymbol{y}) \,\mathrm{d}\boldsymbol{y} \leq C_\gamma := \int_{\mathbb{R}^d} J(\boldsymbol{x}-\boldsymbol{y}) \,\mathrm{d}\boldsymbol{y} < \infty$,
(f) There exists $c_1 > 0$ such that $\varepsilon a + \frac{1}{\varepsilon}W''(u) \geq c_1, \forall u \in \mathbb{R}$.

Let $H^m := H^m(\Omega)$ and $\|\cdot\|_m, m = 0, \pm 1, \cdots$, be the standard Sobolev spaces and their norms, respectively. H^m_{per} is the space of all periodic functions in H^m. In particular, the norm and inner product of $L^2 := H^0$ are denoted by $\|\cdot\|$ and $(\cdot,\cdot)$ respectively. $\star$ represents the convolution operation. If not specified, C is a general constant that may vary depending on the situation and independent of initial value.

Next, we state some elementary inequalities and present some properties of the kernel [1] which will be used in the following part.

Lemma 2.1. *(Young's inequality for the convolution [61]) Assume $f \in L^p(\mathbb{R}^d), g \in L^q(\mathbb{R}^d)$ with $1 \leq p, q \leq \infty$ and $\frac{1}{r} = \frac{1}{p} + \frac{1}{q} - 1 \geq 0$, then $f \star g \in L^r(\mathbb{R}^d)$ and*

$$\|f \star g\|_{L^r(\mathbb{R}^d)} \leq \|f\|_{L^p(\mathbb{R}^d)}\|g\|_{L^q(\mathbb{R}^d)}.$$

Proposition 2.1. *For the kernel $J \in L^1(\mathbb{R}^2)$ satisfying* (a)-(e)*, the following properties hold true:*

(i) *For $\eta > 0$, there exists a family of functions $J_\eta : \mathbb{R}^2 \to \mathbb{R}^+$ satisfying* (a)-(e)*, such that*

$$\|\nabla J_\eta\|_{L^1(\mathbb{R}^2)} \leq C_\eta, \quad \|J - J_\eta\|_{L^1(\mathbb{R}^2)} \leq \eta, \quad C_\eta > 0.$$

(ii) *If $v \in W^{1,p}(\mathbb{R}^2)$, $1 \leq p \leq \infty$, then*

$$J \star v \in W^{1,p}(\mathbb{R}^2).$$

(iii) *The sequence $J_\eta \star v \to J \star v$ converges uniformly in $W^{1,p}(\Omega)$ for any $v \in W^{1,p}(\Omega)$, and the limiting function is continuous, i.e.,*

$$J \star v \in C(\Omega), \quad \forall v \in W^{1,p}(\Omega), \quad 1 \leq p \leq \infty.$$

3. Long-time stability of the continuous problem

In this section, we will study the long-time stability of the continuous model (1.1) in L^2 and H^1 spaces.

3.1. **Long-time stability in L^2.** The L^2 uniform bound of the weak solution of (1.1) has been strictly proven in our previous work [1]. We state this theorem here without proof.

Theorem 3.1 (Uniform estimate in L^2)**.** *Let u be the weak solution of the equation (1.1) with the initial data $u^0 \in L^2$. If $a > \frac{c(\varepsilon\lambda_0+\varepsilon^2+1)}{\varepsilon^2}$ with some constant $c > 0$, then there exist constants $C,\ \theta > 0$, such that*

$$\|u\|^2 \le \exp(-\theta t)\|u^0\|^2 + \frac{C}{\theta}(1-\exp(-\theta t)).$$

Moreover, if $\lambda_0 > \frac{c(\varepsilon^2+1)}{\varepsilon}$, there exists $t_0(\|u^0\|)$ and a constant $M > 0$ independent of u^0, such that

$$\|u\| \le M, \quad \forall t > t_0(\|u^0\|).$$

Theorem 3.1 shows the long-time stability of (1.1) in L^2 norm.

3.2. **Long-time stability in H^1.** In order to prove the long-time stability in H^1 of (1.1), we need Theorem 3.1 and following lemmas.

Lemma 3.2 (The Gagliardo-Nirenberg inequality in bounded domains [62, 63])**.** *Let Ω be a bounded Lipschitz domain. Suppose $v \in L^4(\Omega)$ and $\nabla v \in L^2(\Omega)$, then*

$$\|v\|_{L^4(\Omega)} \le C\,\|\nabla v\|^{\frac{1}{4}}\,\|v\|^{\frac{3}{4}} + C\|v\|, \tag{3.1}$$

where constant $C > 0$ depends on Ω.

Lemma 3.3 (The uniform Grönwall lemma [44])**.** *Let g, h, y on $[t_0, +\infty)$ are three positive local integrable functions, such that y' on $[t_0, +\infty)$ is local integrable, which satisfy that for $t \ge t_0$,*

$$\frac{dy}{dt} \le gy + h, \quad \text{and} \int_t^{t+r} g(s)ds \le a_1, \quad \int_t^{t+r} h(s)ds \le a_2, \quad \int_t^{t+r} y(s)ds \le a_3,$$

where a_1, a_2, a_3, r are positive numbers and r is arbitrarily fixed. Then we have

$$y(t+r) \le \left(\frac{a_3}{r} + a_2\right)\exp(a_1), \quad \forall t \ge t_0. \tag{3.2}$$

To establish the uniform estimate in H^1, we also need the following result on the estimate in H^1 on a finite time interval. The proof follows closely that of [45], therefore we present the result without proof.

Lemma 3.4 (Estimate on a finite interval [45])**.** *Under the same assumptions as in Theorem 3.1, for any given $T > 0$, there exists a constant $M_0 > 0$ depending on u^0, such that*

$$\|u\|_1 \le M_0,\ \forall 0 \le t \le T. \tag{3.3}$$

Now we derive a uniform estimate in H^1.

Theorem 3.2 (Uniform estimate in H^1)**.** *Assume that $\Delta J \in L^1(\Omega)$, $\Delta a \in L^\infty(\Omega)$, and $u^0 \in H^1(\Omega)$. If $a > \frac{d_1(\varepsilon\lambda_0+\varepsilon^2+1)}{\varepsilon^2}$, $\lambda_0 > \frac{d_1(\varepsilon^2+1)}{\varepsilon}$ with some constant $d_1 > 0$, then there exists $t^*(\|u^0\|)$, and a constant $M > 0$ independent of u^0, such that*

$$\|u\|_1 \le M, \quad \forall t \ge t^*(\|u^0\|). \tag{3.4}$$

Proof. Taking the inner product of (1.1) with u, we have

$$\begin{aligned}\frac{1}{2}\frac{d}{dt}\int_\Omega u^2\ \mathrm{d}\boldsymbol{x} &= (\varepsilon\mathcal{L}u, \Delta u) - \frac{1}{\varepsilon}\int_\Omega W''(u)|\nabla u|^2 d\boldsymbol{x} + \lambda_0\int_{\Omega\setminus D} u(f-u)\ \mathrm{d}\boldsymbol{x} \\ &:= T_1 + T_2 + T_3.\end{aligned} \tag{3.5}$$

Using the same techniques as the proof of Theorem 3.1 in [1], we can obtain the following estimates for T_1, T_2 and T_3:

$$T_1 \le -\int_\Omega \varepsilon a|\nabla u|^2\ \mathrm{d}\boldsymbol{x} + \varepsilon\beta_1\|u\|_1^2, \tag{3.6}$$

$$T_2 \le -\frac{\beta_2}{\varepsilon}\||u|\nabla u|\|^2 + \frac{\beta_3}{\varepsilon}\|\nabla u\|^2, \tag{3.7}$$

$$T_3 \le -\frac{\lambda_0}{2\beta_4}\|u\|^2 + \frac{\lambda_0}{4\beta_4^2}\||u|\nabla u|\|^2 + C(\Omega, \lambda_0, f), \tag{3.8}$$

where $\beta_i > 0,\ i = 1, 2, 3, 4$ and $C(\Omega, \lambda_0, f) > 0$ are constants. Taking (3.6)-(3.8) into (3.5) and using Young's inequality, we derive

$$\begin{aligned}\frac{1}{2}\frac{d}{dt}\int_\Omega u^2\ \mathrm{d}\boldsymbol{x} &\le \int_\Omega \varepsilon(-a+\beta_1+\frac{\beta_3}{\varepsilon^2})|\nabla u|^2\ \mathrm{d}\boldsymbol{x} \\ &\quad + (\varepsilon\beta_1 - \frac{\lambda_0}{2\beta_4})\|u\|^2 + (\frac{\lambda_0}{4\beta_4^2} - \frac{\beta_2}{\varepsilon})\||u|\nabla u|\|^2 + C(\Omega, \lambda_0, f) \\ &\le \int_\Omega \varepsilon(-a+\beta_1+\frac{\lambda_0}{4\varepsilon\beta_4}+\frac{\beta_3-\beta_2\beta_4}{\varepsilon^2})|\nabla u|^2\ \mathrm{d}\boldsymbol{x} \\ &\quad + (\varepsilon\beta_1 - \frac{\beta_2\beta_4}{\varepsilon} - \frac{\lambda_0}{4\beta_4})\|u\|^2 + C(\Omega, \lambda_0, f) \\ &\le \int_\Omega \varepsilon(-a+\beta_1+\frac{\lambda_0}{4\varepsilon\beta_4}+\frac{\beta_5}{\varepsilon^2})|\nabla u|^2\ \mathrm{d}\boldsymbol{x} \\ &\quad + (\varepsilon\beta_1 - \frac{\beta_2\beta_4}{\varepsilon} - \frac{\lambda_0}{4\beta_4})\|u\|^2 + C(\Omega, \lambda_0, f),\end{aligned}$$

in which the second inequality holds for $\lambda_0 > \frac{4\beta_4^2\beta_2}{\varepsilon}$ and the third inequality holds for $\beta_5 \ge \max\{0, \beta_3 - \beta_2\beta_4\}$. Let $a > \frac{d_1(\varepsilon\lambda_0+\varepsilon^2+1)}{\varepsilon^2}$, $\lambda_0 > \frac{d_1(\varepsilon^2+1)}{\varepsilon}$ with $d_1 \ge \max\{\beta_1, 4\beta_4\beta_5, \frac{1}{4\beta_4}, 4\beta_2\beta_4, 4\beta_2\beta_4^2\}$, then $A := \varepsilon(a - \beta_1 - \frac{\lambda_0}{4\varepsilon\beta_4} - \frac{\beta_5}{\varepsilon^2}) > 0,\ B := \frac{\lambda_0}{4\beta_4} + \frac{\beta_2\beta_4}{\varepsilon} - \varepsilon\beta_1 > 0$. We thus deduce

$$\frac{d}{dt}\|u\|^2 + A\|\nabla u\|^2 \le C. \tag{3.9}$$

By integrating (3.9) on the interval $[t, t+r]$ for $r > 0$ fixed, we derive

$$A\int_t^{t+r}\|\nabla u(s)\|^2 ds \le Cr + \|u(t)\|^2.$$

For all $t > t_0(\|u^0\|)$, using Theorem 3.1, we have

$$\int_t^{t+r}\|\nabla u(s)\|^2 ds \le \frac{Cr+M}{A}. \tag{3.10}$$

Taking the inner product of (1.1) with $-\Delta u$, and using Young's inequality, we derive

$$\frac{1}{2}\frac{d}{dt}\|\nabla u\|^2 + (\Delta(\varepsilon\mathcal{L}u + \frac{1}{\varepsilon}W'(u)), \Delta u) \le 2\lambda_0\|\nabla u\|^2 + C. \tag{3.11}$$

It remains to estimate $(\Delta(\varepsilon\mathcal{L}(u)+\frac{1}{\varepsilon}W'(u)),\Delta u)$. To simplify the notation, let $h:=\varepsilon au+\frac{1}{\varepsilon}W'(u)$. Then, $(\Delta(\varepsilon\mathcal{L}(u)+\frac{1}{\varepsilon}W'(u)),\Delta u)=(\Delta h,\Delta u)-(\varepsilon\Delta J\star u,\Delta u)$. Using Young's inequality, we deduce

$$\begin{aligned}\int_\Omega \Delta h\Delta u d\boldsymbol{x} \geq& \int_\Omega(\varepsilon a+\frac{1}{\varepsilon}W''(u))(\Delta u)^2 d\boldsymbol{x}-c(\delta_0)\int_\Omega|u\Delta a|^2 d\boldsymbol{x}\\ &-\delta_0\int_\Omega|\Delta u|^2 d\boldsymbol{x}-c(\delta_0)\int_\Omega|\nabla a\cdot\nabla u|d\boldsymbol{x}-\delta_0\int_\Omega|\Delta u|^2 d\boldsymbol{x}\\ &-c(\delta_0)\int_\Omega|W^{(3)}(u)|^2|\nabla u|^4 d\boldsymbol{x}\\ \geq&(c_1-3\delta_0)\int_\Omega|\Delta u|^2 d\boldsymbol{x}-C-C\int_\Omega|\nabla u|^4 d\boldsymbol{x},\end{aligned}\tag{3.12}$$

where constants $c(\delta_0)>0$ and $\delta_0>0$ are associated with Young's inequality and constant c_1 is given in condition (f). Now we estimate $\int_\Omega|\nabla u|^4 d\boldsymbol{x}$. Taking $v=\nabla u$ in the Gagliardo-Nirenberg inequality in bounded domains (3.1), as described in Lemma 3.2, then applying (3.3), yields

$$\|\nabla u\|_{L^4(\Omega)}\leq C\|\Delta u\|^{\frac{1}{4}}\|\nabla u\|^{\frac{3}{4}}+C\|\nabla u\|\leq CM_0\|\Delta u\|^{\frac{1}{4}}+C\|\nabla u\|.\tag{3.13}$$

By using Young's inequality, we have

$$\|\nabla u\|^4_{L^4(\Omega)}\leq\delta_0'\|\Delta u\|^2+c(\delta_0')+C\|\nabla u\|^4,\tag{3.14}$$

where constants $\delta_0'>0$ and $c(\delta_0')>0$ depend on several constants associated with Young's inequality. Inserting (3.14) to (3.12), we get

$$\int_\Omega\Delta h\Delta u d\boldsymbol{x}\geq(c_1-3\delta_0-C\delta_0')\int_\Omega|\Delta u|^2 d\boldsymbol{x}-C\|\nabla u\|^4-C.\tag{3.15}$$

Since $\Delta J\in L^1(\Omega)$, then by using Hölder inequality, Young's inequality and Lemma 2.1, we derive

$$\begin{aligned}\int_\Omega\varepsilon(\Delta J\star u)\Delta u d\boldsymbol{x}\leq&\varepsilon\|\Delta J\star u\|\|\Delta u\|\leq c(\delta_0)\|\Delta J\star u\|^2+\delta_0\|\Delta u\|^2\\ \leq& c(\delta_0)\|\Delta J\|^2_{L^1(\Omega)}\|u\|^2+\delta_0\|\Delta u\|^2\leq\delta_0\|\Delta u\|^2+C,\quad\forall t>t_0(\|u^0\|),\end{aligned}\tag{3.16}$$

in which Lemma 2.1 was used in the third inequality and Theorem 3.1 was utilized in the last inequality. Combining estimates (3.15) and (3.16), we obtain

$$(\Delta(\varepsilon\mathcal{L}(u)+\frac{1}{\varepsilon}W'(u)),\Delta u)\geq(c_1-4\delta_0-C\delta_0')\int_\Omega|\Delta u|^2 d\boldsymbol{x}-C\|\nabla u\|^4-C.\tag{3.17}$$

Taking (3.17) to (3.11), we derive

$$\frac{1}{2}\frac{d}{dt}\|\nabla u\|^2+(c_1-4\delta_0-C\delta_0')\int_\Omega|\Delta u|^2 d\boldsymbol{x}\leq 2\lambda_0\|\nabla u\|^2+C\|\nabla u\|^4+C.$$

Choosing δ_0 and δ_0' be small enough such that $c_1-4\delta_0-C\delta_0'>0$, we have

$$\frac{1}{2}\frac{d}{dt}\|\nabla u\|^2\leq(2\lambda_0+C\|\nabla u\|^2)\|\nabla u\|^2+C.\tag{3.18}$$

Applying the uniform Grönwall lemma 3.3 to (3.18) and utilizing inequality (3.10), we derive

$$\|\nabla u\|^2\leq C(r,\lambda_0),\quad\forall t\geq t^*(\|u^0\|):=t_0(\|u^0\|)+r,\tag{3.19}$$

where $r>0$ is arbitrarily fixed, and $C(r,\lambda_0)$ is independent of u^0. Combining (3.19) with Theorem 3.1, we get (3.4). This completes the proof. □

Theorem 3.2 implies that the problem (1.1) is long time stable in H^1.

4. Long-time stability of the discrete-in-time problem

In order to establish the long-time stability for the temporal discretization of the nonlocal Cahn-Hilliard model, we need to modify the nonlinear potential $W(u)$ by using the truncation technique, which has been frequently used in the literature; see, e.g, [64]. The idea is to replace $W(u)$ by

$$W(u)=\begin{cases}(6L^2-6L+1)u^2+(6L^2-8L^3)u+11L^4+2L^3+5L^2, & u>L,\\ u^2(u-1)^2, & |u|\le L,\\ (6L^2+6L+1)u^2+(16L^3+6L^2+4L)u+11L^4+2L^3+5L^2, & u<-L.\end{cases}\tag{4.1}$$

It can be proved that $W(u)\in C^2(\mathbb{R})$, and $W''(u)$ satisfies the following condition: there exists a constant K such that

$$\max_{u\in\mathbb{R}}|W''(u)|\le K.\tag{4.2}$$

We consider the time semi-discrete scheme based on the convexity splitting method, proposed in [1]. For simplicity, we give a brief introduction of this scheme. E_1 and E_2 in (1.3) are splitted into the sum of a convex and a concave part. Specifically, one can split $E_1=E_{11}-E_{12}$ with

$$E_{11}=\frac{\varepsilon}{2}(\mathcal{L}u,u)+\int_\Omega\frac{P_1}{2}|u|^2\mathrm{d}\boldsymbol{x},\quad E_{12}=\int_\Omega-\frac{1}{\varepsilon}W(u)+\frac{P_1}{2}|u|^2\mathrm{d}\boldsymbol{x},\tag{4.3}$$

andtomn split $E_2=E_{21}-E_{22}$ with

$$E_{21}=\int_\Omega\frac{P_2}{2}|u|^2\mathrm{d}\boldsymbol{x},\quad E_{22}=\int_\Omega-\frac{\lambda}{2}(f-u)^2+\frac{P_2}{2}|u|^2\mathrm{d}\boldsymbol{x}.\tag{4.4}$$

$P_1>\frac{1}{\varepsilon}$ and $P_2>\lambda$ are chosen to ensure that $E_{11},E_{12},E_{21},E_{22}$ are strictly convex. Let $\Delta t=\frac{T}{N},\ t^n=n\Delta t,\ n\le N,\ n,N\in\mathbb{N}$ and u^n be the numerical solution at t^n. Combining (4.3)-(4.4) and applying the forward Euler finite difference method in time, with the nonlocal term treated implicitly and the nonlinear term and fidelity term treated explicitly, we derive a first-order scheme as follows:

$$\frac{u^{n+1}-u^n}{\Delta t}=\varepsilon\Delta\mathcal{L}u^{n+1}+\frac{1}{\varepsilon}\Delta W'(u^n)+P_1\Delta(u^{n+1}-u^n)-P_2(u^{n+1}-u^n)+\lambda(f-u^n).\tag{4.5}$$

Next we analyze the long-time stability of scheme (4.5). We give an equality which will be used frequently:

$$2(a-b,a)=\|a\|^2-\|b\|^2+\|a-b\|^2,\quad a,b\in L^2.\tag{4.6}$$

4.1. Uniquness.

We first show the uniquness of the solution of scheme (4.5), which can be rewritten as

$$(\frac{1}{\Delta t}-\varepsilon\Delta\mathcal{L}-P_1\Delta+P_2)u^{n+1}=\frac{u^n}{\Delta t}+\frac{1}{\varepsilon}\Delta W'(u^n)-P_1\Delta u^n+P_2u^n+\lambda(f-u^n).\tag{4.7}$$

Theorem 4.3. *For every given $v\in H^1_{per}$ and for any $\Delta t>0$, there exists a unique weak solution u of the following equation:*

$$\frac{u}{\Delta t}=\frac{v}{\Delta t}+\varepsilon\Delta\mathcal{L}u+P_1\Delta u-P_2u+\frac{1}{\varepsilon}\Delta W'(v)+\lambda(f-v)-P_1\Delta v+P_2v.\tag{4.8}$$

Proof. The weak formulation of (4.8) is : $\forall\phi\in H^1_{per}$,

$$(\frac{u}{\Delta t},\phi)=(\frac{v}{\Delta t},\phi)+(\varepsilon\Delta\mathcal{L}u+P_1\Delta u-P_2u,\phi)+(\frac{1}{\varepsilon}\Delta W'(v)+\lambda(f-v)-P_1\Delta v+P_2v,\phi).$$

It can be written as:

$$\mathcal{A}(u,\phi)=\mathcal{F}_v(\phi),$$

with

$$\mathcal{A}(u,\phi) = (\frac{u}{\Delta t} - \varepsilon\Delta\mathcal{L}u - P_1\Delta u + P_2 u, \phi),$$
$$\mathcal{F}_v(\phi) = (\frac{v}{\Delta t} + \frac{1}{\varepsilon}\Delta W'(v) + \lambda(f-v) - P_1\Delta v + P_2 v, \phi).$$

It is straightforward that the bilinear form $\mathcal{A}(u,v)$ is continuous and coercive in H^1. $\mathcal{F}_v$ is a linear continuous functional. By using the classical Lax-Milgram theorem, the existence and uniqueness of the weak solution of (4.8) can be proved. □

4.2. **Long-time stability in L^2.** The long-time L^2-stability for the discrete-in-time problem is proved by giving the time uniform bound in L^2 norm under the assumption that $u^0 \in H^1$.

Theorem 4.4 (Time uniform bound in L^2)**.** *Assume $u^0 \in H^1$. If*

$$\lambda_0 > d_2(\varepsilon\|J\|_{W^{1,1}} + 1),\ a > \frac{d_2(K+\varepsilon+\varepsilon^2)}{\varepsilon^2},\ P_1 > \frac{d_2 K}{\varepsilon},\ P_2 > d_2\lambda_0, \tag{4.9}$$

with some constant $d_2 > 0$, then for any $\Delta t > 0$, there exists N^* dependent of $\|u^0\|_1$, and a constant $M > 0$ independent of u^0, such that for all $n \geq N^*$,

$$\|u^n\| \leq M. \tag{4.10}$$

Proof. Taking the inner product of (4.5) with u^{n+1}, we have

$$\begin{aligned}
0 =&(\frac{1}{\Delta t} + P_2)(u^{n+1} - u^n, u^{n+1}) - (\lambda(f-u^n), u^{n+1}) \\
&- (\varepsilon\Delta\mathcal{L}u^{n+1}, u^{n+1}) - (\frac{1}{\varepsilon}\Delta W'(u^n), u^{n+1}) - (P_1\Delta(u^{n+1}-u^n), u^{n+1}) \\
=&((\frac{1}{\Delta t} + P_2 - \lambda)(u^{n+1}-u^n), u^{n+1}) - (\lambda(f-u^{n+1}), u^{n+1}) - (\varepsilon\Delta\mathcal{L}u^{n+1}, u^{n+1}) \\
&+ (\frac{1}{\varepsilon}W''(u^n)\nabla u^{n+1}, \nabla u^{n+1}) + ((P_1 - \frac{1}{\varepsilon}W''(u^n))\nabla(u^{n+1}-u^n), \nabla u^{n+1}) \\
:=&\mathrm{I} + \mathrm{II} + \mathrm{III} + \mathrm{IV} + \mathrm{V}.
\end{aligned} \tag{4.11}$$

Taking the use of (4.6), I and V can be respectively rewritten as:

$$\mathrm{I} = \int_\Omega (\frac{1}{2\Delta t} + \frac{P_2}{2} - \frac{\lambda}{2})(|u^{n+1}|^2 - |u^n|^2 + |u^{n+1}-u^n|^2)d\boldsymbol{x}, \tag{4.12}$$

$$\mathrm{V} = \int_\Omega (\frac{P_1}{2} - \frac{1}{2\varepsilon}W''(u^n))(|\nabla u^{n+1}|^2 - |\nabla u^n|^2 + |\nabla u^{n+1} - \nabla u^n|^2)d\boldsymbol{x}. \tag{4.13}$$

By using the Young's inequality, II can be estimated as:

$$\mathrm{II} \geq \int_\Omega \lambda(-\frac{|f|^2}{2} - \frac{|u^{n+1}|^2}{2} + |u^{n+1}|)d\boldsymbol{x} \geq \int_\Omega \lambda(-\frac{|f|^2}{2} + \frac{|u^{n+1}|^2}{2})d\boldsymbol{x}. \tag{4.14}$$

Now, only III remains to be estimated. Since $\varepsilon(\Delta\mathcal{L}u^{n+1}, u^{n+1}) = -\varepsilon(\nabla(au^{n+1}), \nabla u^{n+1}) + \varepsilon(J \star u^{n+1}, -\Delta u^{n+1})$, then using Hölder inequality and Young's inequality, we have

$$\begin{aligned}
-(\nabla(au^{n+1}), \nabla u^{n+1}) =& -\int_\Omega a|\nabla u^{n+1}|^2\ \mathrm{d}\boldsymbol{x} - \int_\Omega \nabla(a)u^{n+1}\nabla u^{n+1}\ \mathrm{d}\boldsymbol{x} \\
\leq& -\int_\Omega a|\nabla u^{n+1}|^2\ \mathrm{d}\boldsymbol{x} + C_1\|J\|_{W^{1,1}}\|u^{n+1}\|^2 + \frac{\delta_1}{2}\|\nabla u^{n+1}\|^2,
\end{aligned} \tag{4.15}$$

where the general Sobolev inequality was applied in the second estimate and constant $C_1 > 0$ depends on constant $\delta_1 > 0$ associated with Young's inequality and a few constant associated with

the general Sobolev inequality. Since $J\star u$ is periodic, then by utilizing Lemma 2.1 and Proposition 2.1, we find

$$\begin{aligned}(J\star u^{n+1},-\Delta u^{n+1}) &\le |\int_\Omega \nabla(J_\eta\star u^{n+1})(\nabla u^{n+1})d\boldsymbol{x}| + |\int_\Omega \nabla((J-J_\eta)\star u^{n+1})\nabla u^{n+1}d\boldsymbol{x}|\\ &\le \int_\Omega |(\nabla J_\eta\star u^{n+1})(\nabla u^{n+1})|d\boldsymbol{x} + \int_\Omega |((J-J_\eta)\star\nabla u^{n+1})\nabla u^{n+1}|d\boldsymbol{x}\\ &\le \|\nabla J_\eta\|_{L^1}\|u^{n+1}\|\|\nabla u^{n+1}\| + \|J-J_\eta\|_{L^1}\|\nabla u^{n+1}\|^2\\ &\le (\frac{C_\eta\delta_2}{2}+\eta)\|\nabla u^{n+1}\|^2 + \frac{C_\eta}{2\delta_2}\|u^{n+1}\|^2\end{aligned} \tag{4.16}$$

where constant $\delta_2>0$ is associated with Young's inequality. Here, Hölder inequality was applied in the third estimate and Young's inequality was used in the last estimate. Combining (4.15)-(4.16) gives

$$\mathrm{III}\ge\int_\Omega \varepsilon(a-\frac{C_\eta\delta_2}{2}-\frac{\delta_1}{2}-\eta)|\nabla u^{n+1}|^2\,\mathrm{d}\boldsymbol{x} - \varepsilon(\frac{C_\eta}{2\delta_2}+C_1\|J\|_{W^{1,1}})\|u^{n+1}\|^2. \tag{4.17}$$

Inserting (4.12)-(4.17) into (4.11), dropping some unnecessary terms and using the same technique as the estimation of T_3, we obtain

$$\begin{aligned}&(\frac{1}{2\Delta t}+\frac{P_2}{2}-\varepsilon(C_1\|J\|_{W^{1,1}}+\frac{C_\eta}{2\delta_2}))\|u^{n+1}\|^2\\ &+\int_\Omega(\varepsilon a+\frac{P_1}{2}+\frac{1}{2\varepsilon}W''(u^n)-\varepsilon(\frac{\delta_1}{2}+\frac{C_\eta\delta_2}{2}+\eta))|\nabla u^{n+1}|^2d\boldsymbol{x}\\ &\le(\frac{1}{2\Delta t}+\frac{P_2}{2})\|u^n\|^2+\int_\Omega(\frac{P_1}{2}-\frac{1}{2\varepsilon}W''(u^n))|\nabla u^n|^2d\boldsymbol{x}-\frac{\lambda_0}{2}\int_{\Omega\setminus D}|u^n|^2d\boldsymbol{x}+C\\ &\le(\frac{1}{2\Delta t}+\frac{P_2}{2}+C_2-\frac{\lambda_0}{2C})\|u^n\|^2+\int_\Omega(\frac{P_1}{2}+C_2-\frac{1}{2\varepsilon}W''(u^n))|\nabla u^n|^2d\boldsymbol{x}+C,\end{aligned} \tag{4.18}$$

where constant $C_2>0$ depends on a few constants associated with Young's inequality. Denote

$$\begin{aligned}A_0&=\frac{P_2}{2}-\varepsilon(C_1\|J\|_{W^{1,1}}+\frac{C_\eta}{2\delta_2}), & A_1&=\frac{P_2}{2}+C_2-\frac{\lambda_0}{2C},\\ B_0&=\varepsilon a+\frac{P_1}{2}+\frac{1}{2\varepsilon}W''(u^n)-\varepsilon(\frac{\delta_1}{2}+\frac{C_\eta\delta_2}{2}+\eta), & B_1&=\frac{P_1}{2}+C_2-\frac{1}{2\varepsilon}W''(u^n).\end{aligned} \tag{4.19}$$

Dropping the last positive term on the left hand side of (4.18), we get

$$(\frac{1}{2\Delta t}+A_0)\|u^{n+1}\|^2+B_0\|\nabla u^{n+1}\|^2\le(\frac{1}{2\Delta t}+A_1)\|u^n\|^2+B_1\|\nabla u^n\|^2+C. \tag{4.20}$$

Multiplying (4.20) with $2\Delta t$, we have

$$(1+2\Delta tA_0)\|u^{n+1}\|^2+2\Delta tB_0\|\nabla u^{n+1}\|^2\le(1+2\Delta tA_1)\|u^n\|^2+2\Delta tB_1\|\nabla u^n\|^2+C\Delta t. \tag{4.21}$$

Multiplying (4.21) with $\frac{1}{1+2\Delta tA_0}$, we derive

$$\begin{aligned}&\|u^{n+1}\|^2+\frac{2\Delta tB_0}{1+2\Delta tA_0}\|\nabla u^{n+1}\|^2\\ &\le(\frac{1}{1+\frac{2\Delta t(A_0-A_1)}{1+2\Delta tA_1}})(\|u^n\|^2+\frac{2\Delta tB_1}{1+2\Delta tA_1}\|\nabla u^n\|^2)+\frac{C\Delta t}{1+2\Delta tA_0}.\end{aligned} \tag{4.22}$$

Denote $s := \frac{2\Delta t(A_0-A_1)}{1+2\Delta t A_1}$, $c_0 = \frac{(A_0-A_1)}{1+2\Delta t A_1}$. Choosing

$$\begin{aligned} &P_1 > \frac{K}{\varepsilon},\ P_2 > \frac{2\lambda_0}{C} - 4C_2 - \varepsilon(C_1\|J\|_{W^{1,1}} + \frac{C_\eta}{2\delta_2}),\\ &\lambda_0 > 2\varepsilon C C_1\|J\|_{W^{1,1}} + \frac{\varepsilon C C_\eta}{\delta_2} + 2CC_2,\\ &a > \frac{\varepsilon^2(\delta_1 + C_\eta\delta_2 + 2\eta) + \varepsilon(P_1 + 4C_2) + 3K}{2\varepsilon^2}, \end{aligned} \tag{4.23}$$

such that $2A_1 > A_0 > A_1 > 0$ and $B_0 \geq 2B_1 > 0$, then we have $0 < s < 1,\ \forall \Delta t > 0$ and

$$\frac{B_0}{1+2\Delta t A_0} \geq \frac{B_1}{1+2\Delta t A_1},\ \forall \Delta t > 0.$$

Therefore, we can choose $d_2 = \max\{\frac{2}{C},\ 2CC_1,\ \frac{CC_\eta}{\delta_2},\ 2CC_2, \frac{\delta_1+C_\eta\delta_2+2\eta}{2},\ \frac{P_1+4C_2}{2},\ \frac{3}{2}\}$ such that constraint (4.9) satisfies (4.23). Using the fact that $\frac{1}{1+s} \leq \exp(-\frac{s}{2}), \forall s \in (0,1)$ and applying (4.22) for recursion, we deduce

$$\begin{aligned} \|u^{n+1}\|^2 &\leq \frac{1}{1+s}(\|u^n\|^2 + \frac{2\Delta t B_0}{1+2\Delta t A_0}\|\nabla u^n\|^2) + \frac{C\Delta t}{1+2\Delta t A_0}\\ &\leq \exp(-c_0\Delta t)(\|u^n\|^2 + C\|\nabla u^n\|^2) + C\exp(-c_0\Delta t)\Delta t\\ &\leq \exp(-c_0 t^{n+1})(\|u^0\|^2 + C\|\nabla u^0\|^2) + C\sum_{i=0}^{n}\exp(-c_0(t^{i+1}-t^i))\Delta t\\ &\leq \exp(-c_0 t^{n+1})(\|u^0\|^2 + C\|\nabla u^0\|^2) + C\int_0^{t^{n+1}}\exp(-c_0(t^{n+1}-t))dt. \end{aligned}$$

By induction, we have

$$\begin{aligned} \|u^n\|^2 &\leq \exp(-c_0 t^n)(\|u^0\|^2 + C\|\nabla u^0\|^2) + C(1-\exp(-c_0 t^n)))\\ &\leq C\exp(-c_0 t^n)R^2 + C, \end{aligned}$$

where $\|u^0\|_1$ is bounded by a constant R. This implies that there exist a constant M independent of u^0 and $t_0(R) = \frac{1}{c_0}\ln\frac{C}{R^2}$, such that for all $n \geq N^* := \lceil\frac{t_0(R)}{\Delta t}\rceil$,

$$\|u^n\| \leq M,$$

which completes the proof. □

Theorem 4.4 shows that the time semi-discrete scheme (4.5) can preserve the long-time stability of (1.1) in L^2 norm with $u^0 \in H^1$.

4.3. **Long-time stability in H^1.** In order to obtain a discrete counterpart to the uniform bound (3.4), we need the following lemmas.

Lemma 4.5. *Let u^{n+1} be the solution of the numerical scheme (4.5). Then there exist a constant $C_0 > 0$, such that*

$$(1 - C_0\Delta t)\|u^{n+1}\|_1^2 \leq \|u^n\|_1^2 + C\Delta t, \quad \forall \Delta t > 0, \tag{4.24}$$

where $C_0\Delta t < 1, \forall \Delta t > 0$, and A_0, B_0 are defined in (4.19).

Proof. We can infer from (4.20) that

$$(\frac{1}{2\Delta t} + A_0)\|u^{n+1}\|^2 + B_0\|\nabla u^{n+1}\|^2 \leq (\frac{1}{2\Delta t} + A_0 + B_0)\|u^n\|_1^2 + C. \tag{4.25}$$

Dividing both sides of (4.25) by $\frac{1}{2\Delta t}+A_0+B_0$, we get

$$\begin{aligned}&(1-\frac{2\Delta tB_0}{1+2\Delta t(A_0+B_0)})\|u^{n+1}\|^2+(1-\frac{1+2\Delta tA_0}{1+2\Delta t(A_0+B_0)})\|\nabla u^{n+1}\|^2\\&\leq\|u^n\|_1^2+\frac{2\Delta tC}{1+2\Delta t(A_0+B_0)},\\&\leq\|u^n\|_1^2+C\Delta t.\end{aligned}$$

Let $C_0=\max\{\frac{2B_0}{1+2\Delta t(A_0+B_0)},\frac{\frac{1}{\Delta t}+2A_0}{1+2\Delta t(A_0+B_0)}\}$, therefore $C_0\Delta t<1,\forall\Delta t>0$ holds. This completes the proof of Lemma 4.5. □

Corollary 4.1. *For $\|\nabla u^n\|$, there exists a constant $C_0'>0$, such that*

$$(1-C_0'\Delta t)\|\nabla u^{n+1}\|^2\leq\|\nabla u^n\|^2+C\Delta t,\quad\forall\Delta t>0,\tag{4.26}$$

where $C_0'\Delta t<1,\forall\Delta t>0$.

Proof. By applying Poincaré inequality to the right-hand side of (4.25) and using the same argument as in the proof of Theorem 4.4, we can conclude that (4.26) holds. □

Now, we prove that with $u^0\in H^1$, $\|u^n\|_1$ is bounded for all $n\leq N$ for some N.

Lemma 4.6 (Estimate on a finite interval)**.** *Let $T>0$. Under the same conditions as in Theorem 4.4 and assume $0<\Delta t\leq\frac{1}{2C_0}$ with a constant $C_0>0$ in (4.24), then for all $1\leq n\leq N:=\lfloor\frac{T}{\Delta t}\rfloor$, we have*

$$\|u^n\|_1^2\leq C_T(\|u^0\|_1^2+C),\tag{4.27}$$

where constant $C_T>0$ depends on T.

Proof. According to Lemma 4.5, we have

$$\|u^{n+1}\|_1^2\leq\frac{1}{\nu}\|u^n\|_1^2+\frac{1}{\nu}2C\Delta t,\tag{4.28}$$

where $\nu=1-C_0\Delta t>0,\forall\Delta t>0$. Using recursively (4.28), we derive

$$\begin{aligned}\|u^{n+1}\|_1^2&\leq(\frac{1}{\nu})^{n+1}\|u^0\|_1^2+2C\Delta t\sum_{i=1}^{n+1}(\frac{1}{\nu})^i\\&\leq(\frac{1}{\nu})^{n+1}(\|u^0\|_1^2+\frac{2C\Delta t}{1-\nu})\\&\leq(1-C_0\Delta t)^{-(n+1)}(\|u^0\|_1^2+C).\end{aligned}\tag{4.29}$$

Since $C_0\Delta t\leq\frac{1}{2}$, using the fact that $1-x\geq4^{-x},\ \forall x\in(0,\frac{1}{2}]$, we get

$$\|u^n\|_1^2\leq4^{C_0n\Delta t}(\|u^0\|_1^2+C)\leq C_T(\|u^0\|_1^2+C),\ \forall1\leq n\leq N,\tag{4.30}$$

Thus, the lemma is proved. □

To obtain the long-time stability in H^1 norm, we present the following discrete uniform Grönwall lemma; see, e.g., [53].

Lemma 4.7 (The discrete uniform Grönwall lemma)**.** *Given $\Delta t>0$, positive integers n_1,n_2,n_* such that $n_1+n_2+1\leq n_*$, positive sequences ξ^n,ζ^n,η^n such that*

$$\begin{aligned}\Delta t\eta^n&\leq\frac{1}{2},\quad\forall n_1\leq n\leq n_*,\\(1-\Delta t\eta^n)\,\xi^n&\leq\xi^{n-1}+\Delta t\zeta^n,\quad\forall n_1\leq n\leq n_*.\end{aligned}$$

If

$$\Delta t \sum_{n=n_0}^{n_0+n_2} \eta^n \le a_1, \quad \Delta t \sum_{n=n_0}^{n_0+n_2} \zeta^n \le a_2, \quad \Delta t \sum_{n=n_0}^{n_0+n_2} \xi^n \le a_3, \quad \forall n_1 \le n_0 \le n_* - n_2.$$

Then

$$\xi^n \le \left(a_2 + \frac{a_3}{n_2 \Delta t}\right) \exp\left(4a_1\right), \quad \forall n_1 + n_2 + 1 \le n \le n_*.$$

We are now able to prove the long-time H^1-stability for the discrete-in-time problem by giving the time uniform bound in H^1 norm.

Theorem 4.5 (Time uniform bound in H^1)**.** *Let $r \ge r_0$ be arbitrarily fixed and $T_0 = N^* \Delta t$, $N_r = \lfloor \frac{r}{\Delta t} \rfloor$, where constant $r_0 > 0$ is given in (4.47) and constant $N^* > 0$ is given in Theorem 4.4. Under the same conditions as Lemma 4.6 and assume $0 < \Delta t \le \frac{1}{2C_0'}$ with a constant $C_0' > 0$ in (4.26). Then there exists a constant $M_1 > 0$ independent of u^0, such that for all $n \ge N^* + N_r$,*

$$\|u^n\|_1 \le M_1. \tag{4.31}$$

Proof. The main ideal to establish the time uniform bound for $\|u^n\|_1$, $\forall n \ge N^* + N_r$ is as follows:

(i) Applying Lemma 4.6 on $(0, T_0 + r)$, we derive the upper bound for $\|u^n\|_1$, $\forall 1 \le n \le N^* + N_r$. Applying Lemma 4.7, we show that $\|u^{N^*+N_r}\|_1^2 \le M_{**}^2$, where constant $M_{**} > 0$ is given in (4.39) and independent of u^0.

(ii) Iterating Lemmas 4.6 and 4.7, we derive that $\forall i \ge 2$, $\|u^{N^*+(i-1)N_r}\|_1^2 \le M_{**}^2$ and $\|u^n\|_1^2 \le C(\|u^{N^*+(i-1)N_r}\|_1^2)$, where constant $C > 0$ is independent of i and u^0. Thus, we conclude that $\|u^n\|_1 \le M_1$, $\forall n \ge N^* + N_r$, where constant $M_1 > 0$ is given in (4.41) and independent of u^0.

Next, we give a rigorous proof through the following three steps.

Step 1: Applying Lemma 4.6 on $(0, T_0 + r)$, we derive

$$\|u^n\|_1^2 \le C_{T_0+r}(\|u^0\|_1^2 + C). \tag{4.32}$$

We can infer from (4.21) that

$$A_0 \Delta t(\|u^n\|^2 - \|u^{n-1}\|^2) + B_0 \Delta t \|\nabla u^n\|^2 \le B_1 \Delta t \|\nabla u^{n-1}\|^2 + C\Delta t, \tag{4.33}$$

where A_0, B_0, B_1 are defined in (4.19). $A_0 > A_1$, $B_0 \ge 2B_1 > 0$ hold, as shown in the proof of Theorem 4.4. Let $n_1 = N^* + 1$, $n_2 = N_r - 2$. Summing up (4.33) from $n = n_0$ to $n_0 + n_2$, we have

$$\begin{aligned} &A_0 \Delta t(\|u^{n_0+n_2}\|^2 - \|u^{n_0-1}\|^2) + B_0 \Delta t \sum_{n=n_0}^{n_0+n_2} \|\nabla u^n\|^2 \\ &\le B_1 \sum_{n=n_0}^{n_0+n_2} \Delta t \|\nabla u^{n-1}\|^2 + C n_2 \Delta t, \ \forall n_1 \le n_0 \le N^* + N_r - n_2. \end{aligned} \tag{4.34}$$

Inferring from (4.34), we derive

$$\begin{aligned} &A_0 \Delta t \|u^{n_0+n_2}\|^2 + B_1 \Delta t \sum_{n=n_0}^{n_0+n_2} \|\nabla u^n\|^2 \\ &\le B_1 \Delta t \|\nabla u^{n_0-1}\|^2) + A_0 \Delta t \|u^{n_0-1}\|^2 + C n_2 \Delta t. \end{aligned} \tag{4.35}$$

After dropping the first term in (4.35) and dividing by B_1, we arrive to

$$\Delta t \sum_{n=n_0}^{n_0+n_2} \|\nabla u^n\|^2 \le \Delta t \|\nabla u^{n_0-1}\|^2 + \frac{A_0}{B_1} \Delta t \|u^{n_0-1}\|^2 + \frac{C}{B_1} n_2 \Delta t. \tag{4.36}$$

Using estimate (4.32) and Theorem 4.4, we get

$$\begin{aligned}\Delta t\sum_{n=n_0}^{n_0+n_2}\|\nabla u^n\|^2 &\le \Delta t C_{T_0+r}(\|u^0\|_1^2+C)+\frac{A_1\Delta t M^2}{B_1}+\frac{Cn_2\Delta t}{B_1}\\ &\le C(R^2+M^2+n_2\Delta t).\end{aligned}\tag{4.37}$$

Let $r\ge 2(R^2+M^2+\Delta t)$ be arbitrarily fixed. Since $C_0'\Delta t\le\frac{1}{2}$, then applying Lemma 4.7 to (4.26), we have

$$\begin{aligned}\|\nabla u^{N^*+N_r}\|^2 &\le (Cr+\frac{C(M^2+R^2+n_2\Delta t)}{n_2\Delta t})\exp(4Cr)\\ &\le (Cr+C(1+\frac{M^2+R^2}{2(M^2+R^2)}))\exp(Cr)\\ &\le C(r+\frac{3}{2})\exp(Cr):=M_*^2,\end{aligned}\tag{4.38}$$

where constant $M_*>0$ is independent of u^0. Using Theorem 4.4, we arrive at

$$\|u^{N^*+N_r}\|_1^2\le M^2+M_*^2:=M_{**}^2,\tag{4.39}$$

where constant $M_{**}>0$ is independent of u^0. Taking $u^{N^*+N_r}$ as the initial data and applying Lemma 4.6 with $T=r$, we derive

$$\|u^n\|_1^2\le C_r(\|u^{N^*+N_r}\|_1^2+C),\ \forall N^*+N_r+1\le n\le N^*+2N_r.\tag{4.40}$$

Combining (4.40) with (4.39), we obtain

$$\|u^n\|_1^2\le C_r(M_{**}^2+C):=M_1^2,\ \forall N^*+N_r+1\le n\le N^*+2N_r,\tag{4.41}$$

where constant $M_1>0$ is independent of u^0.

Step 2: Let $n_1=N^*+N_r+1,\ n_2=N_r-2$. Summing up (4.26) from $n=n_0$ to n_0+n_2, using estimates (4.39)-(4.41) and Theorem 4.4, we obtain

$$\begin{aligned}\Delta t\sum_{n=n_0}^{n_0+n_2}\|\nabla u^n\|^2 &\le \Delta t\|\nabla u^{n_0-1}\|^2+\frac{A_1\Delta t}{B_1}\|u^{n_0-1}\|^2+\frac{Cn_2\Delta t}{B_1}\\ &\le \Delta t C_r(\|u^{N^*+N_r}\|_1^2+C)+C(M^2+n_2\Delta t)\\ &\le C(M_1^2+M^2+n_2\Delta t),\ \forall n_1\le n_0\le N^*+N_r-n_2.\end{aligned}\tag{4.42}$$

Let $r\ge 2(M_1^2+M^2+\Delta t)$ be arbitrarily fixed. Using Lemma 4.7 on (4.26), we have

$$\begin{aligned}\|\nabla u^{N^*+2N_r}\|^2 &\le (Cr+\frac{C(M_1^2+M^2+n_2\Delta t)}{n_2\Delta t})\exp(4Cr)\\ &\le (Cr+C(1+\frac{M^2+M_1^2}{2(M^2+M_1^2)}))\exp(Cr)\\ &\le C(r+\frac{3}{2})\exp(Cr):=M_*^2.\end{aligned}\tag{4.43}$$

Using Theorem 4.4, we have

$$\|u^{N^*+2N_r}\|_1^2\le M^2+M_*^2:=M_{**}^2.\tag{4.44}$$

As before, taking $u^{N^*+2N_r}$ as initial data and using Lemma 4.6 with $T=r$, we have

$$\|u^n\|_1^2\le C_r(\|u^{N^*+N_r}\|_1^2+C),\ \forall N^*+2N_r+1\le n\le N^*+3N_r.\tag{4.45}$$

Then we derive

$$\|u^n\|_1^2\le M_1^2,\ \forall N^*+2N_r+1\le n\le N^*+3N_r.\tag{4.46}$$

Step 3: Let

$$r_0 = \max\{2(M_1^2 + M^2 + \Delta t), 2(M_1^2 + R^2 + \Delta t)\}. \tag{4.47}$$

Taking $r \geq r_0$, repeating the same procedure as **Step 1** and **Step 2**, for all $n = N^* + (i-1)N_r + 1, \cdots, N^* + iN_r,\ \forall i \geq 2$, we derive that

$$\|u^{N^*+iN_r}\|_1^2 \leq M_{**}^2, \tag{4.48}$$

and

$$\|u^n\|_1^2 \leq C_r(\|u^{N^*+iN_r}\|_1^2 + C),\ \forall N^* + (i-1)N_r + 1 \leq n \leq N^* + iN_r. \tag{4.49}$$

Note that constants $C_r > 0$ and $C > 0$ are independent of i and u^0, then we conclude that

$$\|u^n\|_1^2 \leq M_1^2,\ \forall N^* + (i-1)N_r + 1 \leq n \leq N^* + iN_r. \tag{4.50}$$

This ends the proof of Theorem 4.5. □

According to Theorem 4.5, the time uniform estimates for $\|u^n\|_1$ is independent of $u^0 \in H^1$. It reveals that the discrete problem (4.5) preserves the long-time stability of the continuous problem in H^1 norm.

Remark 4.1. *For the traditional Cahn-Hilliard equation, there exist the H^2 and higher order estimates for certain numerical schemes [65, 66]. However, as far as we know there does not exist such estimates in the literature for the nonlocal Cahn-Hilliard model considered here. By following the work [29], some kind of estimates in fractional Sobolev norm H^γ for γ between 1 and 2 may be considered. However, it is notable that the nonlocal operator used in the current paper differs from the one studied in [29].*

Remark 4.2. *Higher order schemes can also be constructed and analyzed, and uniform-in-time estimates could be obtained in a way similar to the first order scheme. Note that there exist several second order schemes for the non-local Cahn-Hilliard equation, see, e.g., [21, 67, 68], in which the energy stability and local-in-time estimates have been established. However, we would like to emphasize that the accuracy in time of the proposed numerical scheme is not our main concern since we are only interested at the steady-state solution of the model, i.e., the inpainted image.*

5. Numerical experiments

In this section, we test the numerical long-time stability and validate the efficiency of the proposed model in signal reconstruction and image inpainting. We choose the Gaussian kernel function for the nonlocal operator, which satisfies the assumptions in this paper, as follows

$$J_\delta(\boldsymbol{x}) := \frac{\alpha}{(2\pi)^{d/2}\delta^d} \mathrm{e}^{-\frac{|\boldsymbol{x}|^2}{2\delta^2}}, \quad \boldsymbol{x} \in \mathbb{R}^d, \delta > 0, \tag{5.1}$$

where δ and α govern the spatial reach and the magnitude of J_δ, respectively. The kernel satisfies the following conditions:

$$\int_{\mathbb{R}^d} J_\delta(\boldsymbol{x}) \mathrm{d}\boldsymbol{x} = \alpha, \quad \int_{\mathbb{R}^d} J_\delta(\boldsymbol{x})|\boldsymbol{x}|^2 \, \mathrm{d}\boldsymbol{x} = \alpha\delta^{2d}.$$

The degraded image f of a clean image u is generated by a mask function χ of damaged domain D, and a uniformly randomly distributed noise σ:

$$f = \chi u + (1-\chi)\sigma. \tag{5.2}$$

We denote Ratio $= \frac{|D|}{|\Omega|}$ as the damage ratio.

5.1. **Example 1: Validation of long time stability.** To verify that the time uniform estimates are independent of the initial data, we provide a set of initial values for one-dimensional examples as follows:

- Initial value I: $u(x,0) = 10\sin(\pi x)$;
- Initial value II: $u(x,0) = \cos(\pi x) + \sin(\pi x)$;
- Initial value III: $u(x,0) = x(x-\pi)\sin(x)$;
- Initial value IV: $u(x,0) = sin(\pi x)cos(\pi x)$;
- Initial value V: $u(x,0) = \cos(\pi x)$.

Parameters are set as: $\Omega = [0,2]$, $\varepsilon = 0.1, \lambda_0 = 10^9, \alpha = 4\times 10^5, \delta = 6.25\times 10^{-2}, P_1 = \frac{10}{\varepsilon}, P_2 = 1.25\lambda_0, \Delta t = 1$. 1024 Fourier modes are used. We observe the long-time behaviors with different initial data in Example 1A and give an application in signal reconstruction in Example 1B.

Example 1A: Long-time effect of damage severity. Let $u(x) = \sin(\pi x)$. The degraded function $f(x)$ is generated by (5.2). Let $u_i, i = 1, 2, \cdots, 5$ be the numerical solution with initial values I-V.

We performed with Ratio $= \frac{1}{16}, \frac{1}{32}, \frac{1}{64}, \frac{1}{128}$ to investigate the influence. As shown in Figures 1-4, after a long enough time, $u_i, i = 1, 2, \cdots, 5$ tends to nearly the same final state under L^2 and H^1 norms, respectively. Additionally, it is worth noting that as the damaged area decreases, the time required to reach a stable solution also decreases.

To have clear observations of the discrepancy of numerical solutions with different initial values, we calculate the discrepancies in L^2 and H^1 norms, respectively. We define the discrepancies as: $|e|_i = |\|u_i\|_0 - \|u_1\|_0|, |E|_i = |\|u_i\|_1 - \|u_1\|_1|, i = 2, \cdots, 5$.

In Table 1-2, we present the discrepancy in L^2 and H^1 norms, with the Ratio ranging from $\frac{1}{128}$ to $\frac{1}{16}$. We can see all the values are below 10^{-6}, and the value decreases as the Ratio reduces. Precisely, the difference in the L^2 norm is $O(10^{-8})$ for Ratio $= \frac{1}{16}$, and $O(10^{-12})$ for smaller Ratio. Meanwhile, the difference in H^1 norm is $O(10^{-8})$ for Ratio $= \frac{1}{16}$, and $O(10^{-9})$ for the others. These numerical results strongly support the long-time L^2 and H^1 stability of scheme (4.7), as analysed in the previous section.

Also, we plot the degraded functions with Ratio $= \frac{1}{16}, \frac{1}{128}$ in Figure 5, representing the maximum and minimum ratio of damage, respectively. The corresponding inpainted results are shown in Figure 6. Every solution of different initial values converges well to the exact solution. In conclusion, regardless of the initial damage ratio, a sufficiently prolonged inpainting process leads to consistent outcomes.

Ratio	1/16	1/32	1/64	1/128
$\|e\|_2$	4.29E-8	1.15E-12	1.37E-12	1.04E-12
$\|e\|_3$	7.49E-8	1.23E-12	1.63E-12	1.03E-12
$\|e\|_4$	1.45E-9	1.17E-12	1.17E-12	1.16E-12
$\|e\|_5$	4.30E-8	1.27E-12	1.49E-12	1.16E-12

TABLE 1. (Example 1A.) The discrepancy between $\|u_i\|$ and $\|u_1\|$.

Ratio	1/16	1/32	1/64	1/128
$\|E\|_2$	2.09E-8	3.80E-9	3.92E-9	2.60E-10
$\|E\|_3$	1.56E-7	3.43E-9	3.89E-9	2.58E-10
$\|E\|_4$	1.37E-8	4.38E-9	4.35E-9	2.89E-10
$\|E\|_5$	1.87E-8	4.24E-9	4.35E-9	2.89E-10

TABLE 2. (Example 1A.) The discrepancy between $\|u_i\|_1$ and $\|u_1\|_1$.

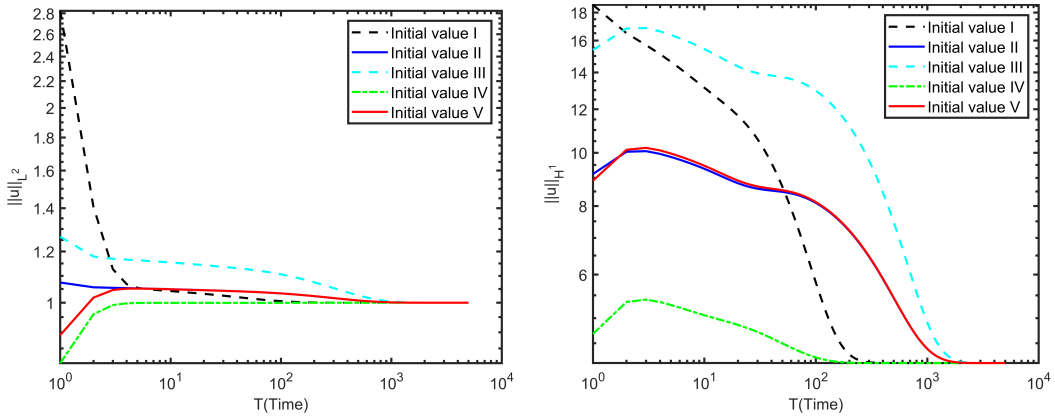

FIGURE 1. (Example 1A.) $\|u\|$(left) and $\|u\|_1$(right) for different initial data with Ratio $= \frac{1}{16}$.

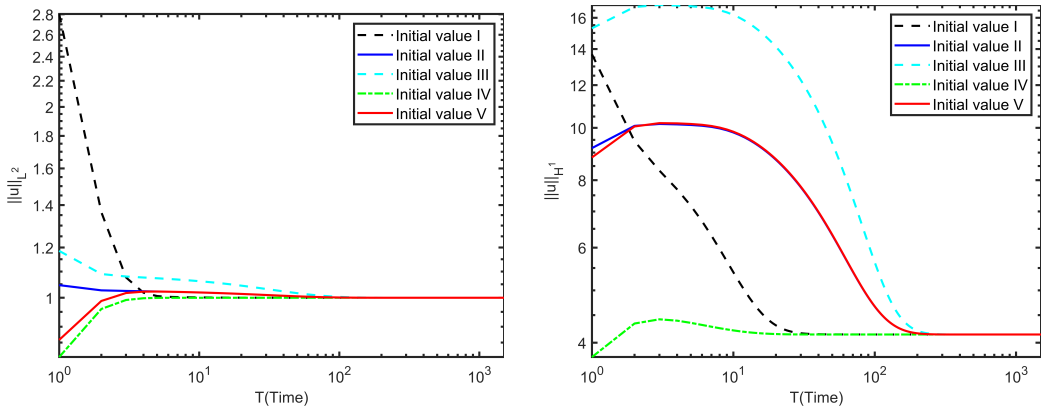

FIGURE 2. (Example 1A.) $\|u\|$(left) and $\|u\|_1$(right) for different initial data with Ratio $= \frac{1}{32}$.

Example 1B: Signal reconstruction. We apply our model to deal with the signal reconstruction problem [69]. A piece-wise constant function is taken as the original signal, its corresponding degraded function is with a damage ratio of $\frac{1}{16}$, as shown in Figure 7. We inpaint the damaged signal with the same initial values as in Example 1A, results are shown in the right of Figure 7, each inpainted signal fits well with the original signal. In Figure 8, we can see that after long enough time $T > 10^3$, each solution coincides under the L^2 and H^1 norms, respectively. And the solutions keep stable till $T = 4 \times 10^4$. This demonstrates that the nonlocal model can effectively capture discontinuous stationary solutions, which is consistent with the conclusions in [26, 70, 71].

5.2. **Example 2: Application of image inpainting.** We apply our nonlocal Cahn-Hilliard inpainting model in two-dimensional image inpainting. The size of an image consists of the rows and columns of pixels and the number of channels, denoted by $M_1 \times M_2 \times Q$. More precisely, for grayscale images, $Q = 1$, and for color images, $Q = 3$.

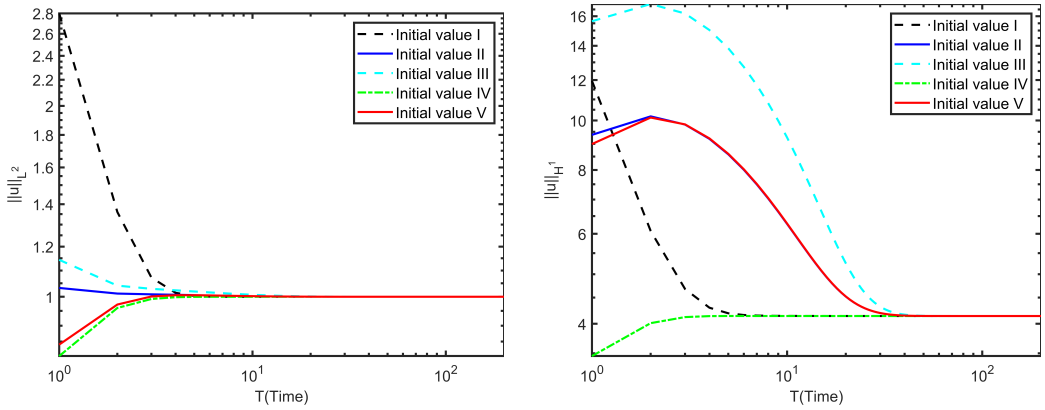

FIGURE 3. (Example 1A.) $\|u\|$ (left) and $\|u\|_1$ (right) for different initial data with Ratio $= \frac{1}{64}$.

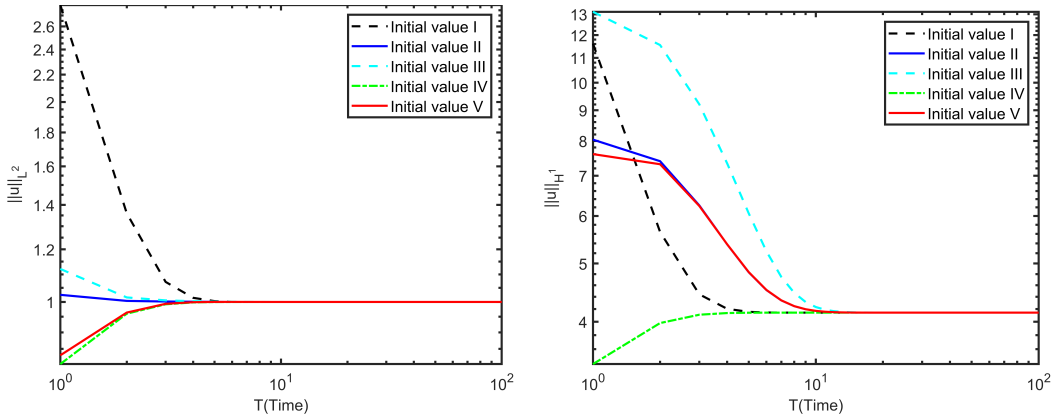

FIGURE 4. (Example 1A.) $\|u\|$ (left) and $\|u\|_1$ (right) for different initial data with Ratio $= \frac{1}{128}$.

We measure the inpainting quality by comparing the degraded image f and the clean image u under the following two metrics [72]:

$$\mathrm{PSNR}(f,u) = 10log_{10}(\frac{M_1 M_2}{\sum_{i=1}^{M_1}\sum_{j=1}^{M_2}(f_{ij}-u_{ij})^2}),$$
$$\mathrm{SSIM}(f,u) = \frac{(2\mu_f\mu_u + B_1)(2\sigma_f\sigma_u + B_2)(\sigma_{fu} + B_3)}{(\mu_f^2+\mu_u^2+B_1)(\sigma_f^2+\sigma_u^2+B_2)(\sigma_f\sigma_u+B_3)},$$

where μ_f is the pixel sample mean of the image f, σ_f is the variance of f, σ_{fu} are the covariance of f and u. Constants B_1, B_2 and B_3 are introduced to avoid divisions by zero. Normally, $B_1 = (D_1L)^2, B_2 = (D_2L)^2, B_3 = \frac{B_2}{2}$. By default, $D_1 = 0.01, D_2 = 0.03$. The pixel-values have a dynamic range of $L = 1$. For colored images, SSIM is calculated by the average of three channels.

Taking a given clean image as the conference, we compare the initial and final values of PSNR and SSIM to assess the inpainting quality, which corresponds to the damaged and the inpainting image. Higher values indicate better image quality.

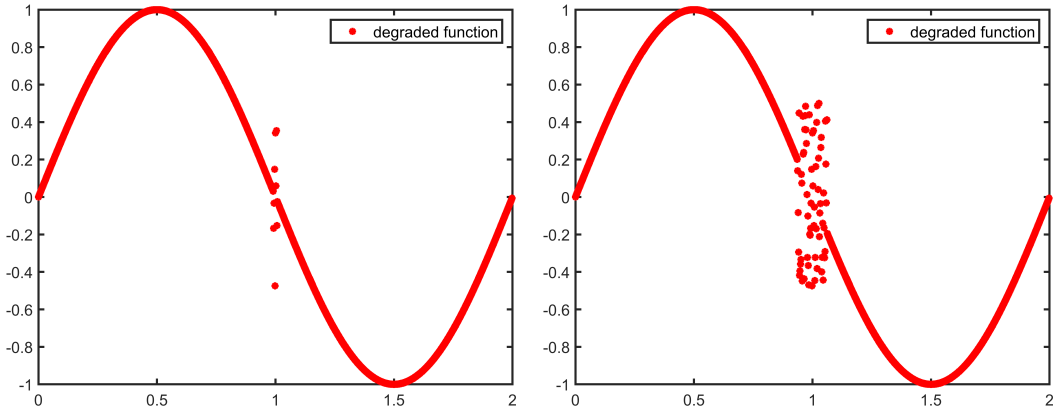

FIGURE 5. (Example 1A.) The degraded functions $f(x)$ with Ratio $= \frac{1}{128}$ (left) and $\frac{1}{16}$ (right).

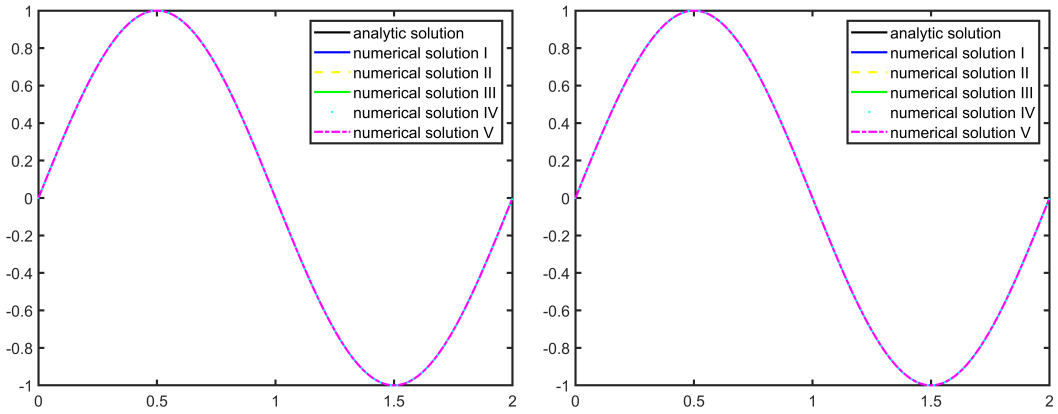

FIGURE 6. (Example 1A.) The inpainted functions $u(x)$ with Ratio $= \frac{1}{128}$ (left) and Ratio $= \frac{1}{16}$ (right).

We adopt a two-stage strategy during the inpainting process as proposed in [14], where the image is firstly repaired with a larger $\varepsilon = \varepsilon_1$ in the first stage until the tolerance is reached, and then improved with a smaller $\varepsilon = \varepsilon_2$ to sharpen the edge in the second stage. The time step size is set by $\Delta t = 1$. The number of Fourier modes N is taken to be equivalent to the image size. The total time for all the experiments is $T = 4 \times 10^3$, with the first stage lasting 3×10^3 and the second stage lasting 10^3. We compare the solutions at $T = 4 \times 10^3, 5 \times 10^3$ with the damaged and clean image to validate the reliability and stability of our method under long-time evolution.

Example 2A: Binary image inpainting. We inpaint three binary images with different shapes and sizes of damaged areas, as shown in Figure 9. We set $\lambda_0 = 5 \times 10^5, \varepsilon_1 = 0.2, \varepsilon_2 = 8 \times 10^{-3}, \delta = 200, \alpha = 1.5 \times 10^5, P_1 = 300, P_2 = 3\lambda_0$.

Table 3 lists the initial and final values of PSNR and SSIM for three images, respectively. It is seen that the values increase after the inpainting process, which indicates that all the images are well-restored.

It is evident from Figure 9 that all the binary images are effectively and well-restored in terms of preserving sharper edges. They also restore the topological transitions well. Particularly, the

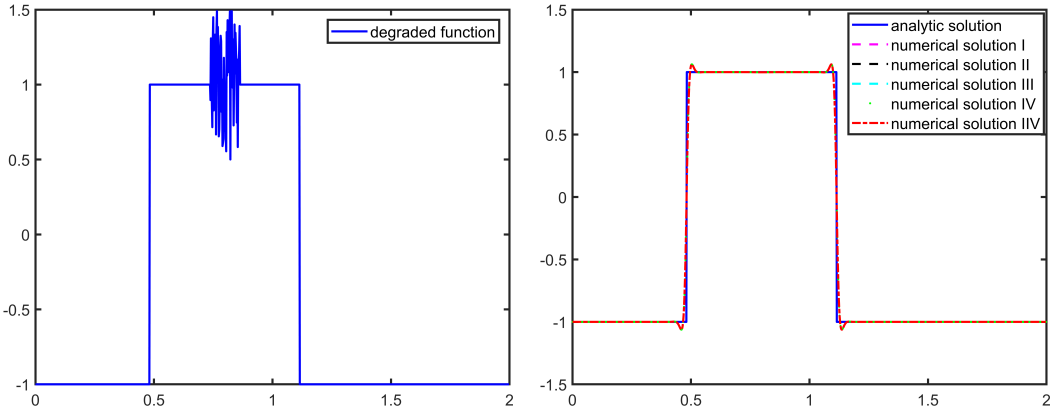

FIGURE 7. (Example 1B.) The damaged signal (left) and the inpainted signals (right) for different initial data with Ratio $= \frac{1}{16}$.

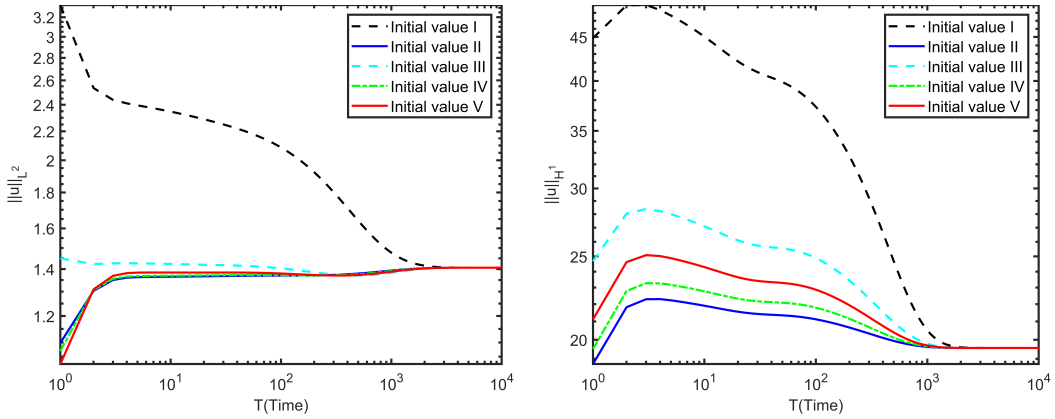

FIGURE 8. (Example 1B.) $\|u\|$ (left) and $\|u\|_1$ (right) for different initial data.

Image	PSNR		SSIM	
	Initial	Final	Initial	Final
Single stripe	13.1681	65.7440	0.7335	0.9996
Jet	20.4123	30.7827	0.9512	0.9927
Eastern cottontail	16.3031	25.3937	0.7710	0.9829

TABLE 3. (Example 2A.) Numerical results for binary images.

Single stripe image has the highest value than the other images due to its simplest structure. We can see from Figure 9(a) that Single stripe is effectively restored in terms of topological transitions, while the other two binary images slightly lose information, as shown in the corner of Jet in Figure 9(b) and the Eastern cottontail's forefoot in Figure 9(c), respectively. The last two columns of Figure 9 imply that the images have already been restored at $T = 4 \times 10^3$, and maintain this state till $T = 5 \times 10^3$, this observation confirms that our method is stable over a long duration.

Example 2B: Grayscale and colored image inpainting. Finally, we present the inpainting results of grayscale and colored images, as shown in Figure 10. We solve the complex Ginzburg-Landau equation and only take the real component of the solution as the inpainted image. The

(a) Comparison results of Single stripe

(b) Comparison results of Jet

(c) Comparison results of Eastern cottontail

FIGURE 9. (Example 2A.) Comparison results of binary images. From left to right: degraded image, clean image, and inpainted image at $T = 4 \times 10^3, 5 \times 10^3$ respectively.

Image	PSNR		SSIM	
	Initial	Final	Initial	Final
Study	21.9767	40.9819	0.9466	0.9951
Cameramen	18.8829	35.3876	0.8088	0.9806
Peppers	19.6356	34.3402	0.8816	0.9608
Building	17.2335	28.0597	0.8693	0.9451

TABLE 4. (Example 2B.) Numerical results for grayscale and colored images.

parameters are given by: $\lambda_0 = 10^9, \varepsilon_1 = 5 \times 10^{-2}, \varepsilon_2 = 8 \times 10^{-3}, \delta = 0.02, \alpha = 10^5, P_1 = \frac{3}{\varepsilon_2}, P_2 = 3\lambda_0$.

We observe from Table 4 that all the inpainted images have high PSNR and SSIM. The Study image has the highest value, and the Building image has the lowest. That is due to the same reason as in Example 2A: the complexity of the damage structure. Illustrated by Figure 10, at $T = 4\times10^3$, all the images are already well-restored in terms of topological connection, and maintain this state till $T = 5 \times 10^3$.

(a) Comparison results of Study

(b) Comparison results of Cameramen man

(c) Comparison results of Peppers

(d) Comparison results of Building

FIGURE 10. (Example 2B.) Comparison results of grayscale and colored images. From left to right: degraded image, clean image and inpainted image at $T = 4 \times 10^3, 5 \times 10^3$ respectively.

6. Concluding remarks

In this paper, we have investigated the long time behavior of the nonlocal Cahn-Hilliard inpainting model introduced in [1]. Precisely, we have established the long time stability of the both continuous problem and its discrete counterpart. This was done by proving the time uniform bounds of the continuous and discrete solutions in L^2 and H^1 norms. Several numerical examples were provided to verify the stability of the proposed model and the efficiency of the numerical method constructed for the model.

References

[1] Dandan Jiang, Mejdi Azaiez, Alain Miranville, and Chuanju Xu. Nonlocal Cahn-Hilliard type model for image inpainting. *Computers & Mathematics with Applications*, 159:76–91, 2024.

[2] Marcelo Bertalmio, Guillermo Sapiro, Vincent Caselles, and Coloma Ballester. Image inpainting. In *Proceedings of the 27th annual conference on Computer graphics and interactive techniques*, pages 417–424, 2000.

[3] Leonid I Rudin and Stanley Osher. Total variation based image restoration with free local constraints. In *Proceedings of 1st international conference on image processing*, volume 1, pages 31–35. IEEE, 1994.

[4] Jianhong Shen and Tony Chan. Variational restoration of nonflat image features: Models and algorithms. *SIAM Journal on Applied Mathematics*, 61(4):1338–1361, 2001.

[5] Tony F Chan and Jianhong Shen. Nontexture inpainting by curvature-driven diffusions. *Journal of visual communication and image representation*, 12(4):436–449, 2001.

[6] Jianhong Shen, Sung Ha Kang, and Tony F Chan. Euler's elastica and curvature-based inpainting. *SIAM journal on Applied Mathematics*, 63(2):564–592, 2003.

[7] Selim Esedoglu and Jianhong Shen. Digital inpainting based on the Mumford–Shah–Euler image model. *European Journal of Applied Mathematics*, 13(4):353–370, 2002.

[8] Tony F Chan and Jianhong Shen. *Image processing and analysis: variational, PDE, wavelet, and stochastic methods*. SIAM, 2005.

[9] Charles M Elliott and SA Smitheman. Numerical analysis of the TV regularization and H^{-1} fidelity model for decomposing an image into cartoon plus texture. *IMA Journal of Numerical Analysis*, 29(3):651–689, 2009.

[10] Abdul Halim and BV Rathish Kumar. An anisotropic PDE model for image inpainting. *Computers & Mathematics with Applications*, 79(9):2701–2721, 2020.

[11] Jireh Jam, Connah Kendrick, Kevin Walker, Vincent Drouard, Jison Gee-Sern Hsu, and Moi Hoon Yap. A comprehensive review of past and present image inpainting methods. *Computer vision and image understanding*, 203:103147, 2021.

[12] John W Cahn and John E Hilliard. Free energy of a nonuniform system. I. Interfacial free energy. *The Journal of chemical physics*, 28(2):258–267, 1958.

[13] Andrea Bertozzi, Selim Esedoglu, and Alan Gillette. Analysis of a two-scale Cahn–Hilliard model for binary image inpainting. *Multiscale Modeling & Simulation*, 6(3):913–936, 2007.

[14] Andrea L Bertozzi, Selim Esedoglu, and Alan Gillette. Inpainting of binary images using the Cahn–Hilliard equation. *IEEE Transactions on image processing*, 16(1):285–291, 2006.

[15] Martin Burger, Lin He, and Carola-Bibiane Schönlieb. Cahn–Hilliard inpainting and a generalization for grayvalue images. *SIAM Journal on Imaging Sciences*, 2(4):1129–1167, 2009.

[16] Wenli Yang, Zhongyi Huang, and Wei Zhu. Image segmentation using the Cahn–Hilliard equation. *Journal of Scientific Computing*, 79:1057–1077, 2019.

[17] Laurence Cherfils, Hussein Fakih, and Alain Miranville. On the Bertozzi–Esedoglu–Gillette–Cahn–Hilliard equation with logarithmic nonlinear terms. *SIAM Journal on Imaging Sciences*, 8(2):1123–1140, 2015.

[18] Andrej Novak and Nora Reinić. Shock filter as the classifier for image inpainting problem using the Cahn-Hilliard equation. *Computers & Mathematics with Applications*, 123:105–114, 2022.

[19] Antoni Buades, Bartomeu Coll, and Jean-Michel Morel. Image denoising methods. A new nonlocal principle. *SIAM review*, 52(1):113–147, 2010.

[20] Zhen Guan, John S Lowengrub, Cheng Wang, and Steven M Wise. Second order convex splitting schemes for periodic nonlocal Cahn–Hilliard and Allen–Cahn equations. *Journal of*

Computational Physics, 277:48–71, 2014.

[21] Qiang Du, Lili Ju, Xiao Li, and Zhonghua Qiao. Stabilized linear semi-implicit schemes for the nonlocal Cahn–Hilliard equation. *Journal of Computational Physics*, 363:39–54, 2018.

[22] Xiao Li, Zhonghua Qiao, and Cheng Wang. Convergence analysis for a stabilized linear semi-implicit numerical scheme for the nonlocal Cahn–Hilliard equation. *Mathematics of Computation*, 90(327):171–188, 2021.

[23] Qiang Du, Max Gunzburger, Richard B Lehoucq, and Kun Zhou. A nonlocal vector calculus, nonlocal volume-constrained problems, and nonlocal balance laws. *Mathematical Models and Methods in Applied Sciences*, 23(03):493–540, 2013.

[24] Qiang Du, Max Gunzburger, Richard B Lehoucq, and Kun Zhou. Analysis and approximation of nonlocal diffusion problems with volume constraints. *SIAM review*, 54(4):667–696, 2012.

[25] Marta D'Elia, Qiang Du, Christian Glusa, Max Gunzburger, Xiaochuan Tian, and Zhi Zhou. Numerical methods for nonlocal and fractional models. *Acta Numerica*, 29:1–124, 2020.

[26] Qiang Du and Jiang Yang. Asymptotically compatible Fourier spectral approximations of nonlocal Allen–Cahn equations. *SIAM Journal on Numerical Analysis*, 54(3):1899–1919, 2016.

[27] Qiang Du and Jiang Yang. Fast and accurate implementation of Fourier spectral approximations of nonlocal diffusion operators and its applications. *Journal of Computational Physics*, 332:118–134, 2017.

[28] Jie Shen, Jie Xu, and Jiang Yang. A new class of efficient and robust energy stable schemes for gradient flows. *SIAM Review*, 61(3):474–506, 2019.

[29] Olena Burkovska and Max Gunzburger. On a nonlocal Cahn–Hilliard model permitting sharp interfaces. *Mathematical Models and Methods in Applied Sciences*, 31(09):1749–1786, 2021.

[30] Mark Ainsworth and Zhiping Mao. Analysis and approximation of a fractional Cahn–Hilliard equation. *SIAM Journal on Numerical Analysis*, 55(4):1689–1718, 2017.

[31] Fangying Song, Chuanju Xu, and George Em Karniadakis. A fractional phase-field model for two-phase flows with tunable sharpness: algorithms and simulations. *Computer Methods in Applied Mechanics and Engineering*, 305:376–404, 2016.

[32] Anna Lischke, Guofei Pang, Mamikon Gulian, Fangying Song, Christian Glusa, Xiaoning Zheng, Zhiping Mao, Wei Cai, Mark M Meerschaert, Mark Ainsworth, et al. What is the fractional Laplacian? A comparative review with new results. *Journal of Computational Physics*, 404:109009, 2020.

[33] Jessica Bosch and Martin Stoll. A fractional inpainting model based on the vector-valued Cahn–Hilliard equation. *SIAM Journal on Imaging Sciences*, 8(4):2352–2382, 2015.

[34] Qiang Liu, Zhiguang Zhang, and Zhichang Guo. On a fractional reaction–diffusion system applied to image decomposition and restoration. *Computers & Mathematics with Applications*, 78(5):1739–1751, 2019.

[35] Antun Lovro Brkić, Darko Mitrović, and Andrej Novak. On the image inpainting problem from the viewpoint of a nonlocal Cahn-Hilliard type equation. *Journal of Advanced Research*, 25:67–76, 2020.

[36] Min Zhang and Guo-Feng Zhang. Fast image inpainting strategy based on the space-fractional modified Cahn-Hilliard equations. *Computers & Mathematics with Applications*, 102:1–14, 2021.

[37] Zhen Guan, Cheng Wang, and Steven M Wise. A convergent convex splitting scheme for the periodic nonlocal Cahn-Hilliard equation. *Numerische Mathematik*, 128(2):377–406, 2014.

[38] Jean E Taylor and John W Cahn. Linking anisotropic sharp and diffuse surface motion laws via gradient flows. *Journal of Statistical Physics*, 77:183–197, 1994.

[39] Francesco Della Porta and Maurizio Grasselli. Convective nonlocal Cahn-Hilliard equations with reaction terms. *arXiv preprint arXiv:1406.1684*, 2014.

[40] Xiaoming Wang. Approximation of stationary statistical properties of dissipative dynamical systems: time discretization. *Mathematics of Computation*, 79(269):259–280, 2010.

[41] Mickaël D Chekroun and Nathan E Glatt-Holtz. Invariant measures for dissipative dynamical systems: Abstract results and applications. *Communications in Mathematical Physics*, 316(3):723–761, 2012.

[42] Jie Jiang, Hao Wu, and Songmu Zheng. Well-posedness and long-time behavior of a non-autonomous Cahn–Hilliard–Darcy system with mass source modeling tumor growth. *Journal of Differential Equations*, 259(7):3032–3077, 2015.

[43] J.C. Simo and F. Armero. Unconditional stability and long-term behavior of transient algorithms for the incompressible Navier-Stokes and Euler equations. *Computer Methods in Applied Mechanics and Engineering*, 111(1-2):111–154, 1994.

[44] Roger Temam. *Infinite-dimensional dynamical systems in mechanics and physics*, volume 68. Springer Science & Business Media, 2012.

[45] Annalisa Iuorio and Stefano Melchionna. Long-time behavior of a nonlocal Cahn-Hilliard equation with reaction. *Discrete and Continuous Dynamical Systems*, 38(8):3765–3788, 2018.

[46] Alain Miranville. *The Cahn–Hilliard equation: recent advances and applications*. SIAM, 2019.

[47] Giulio Schimperna and Hao Wu. On a Class of Sixth-Order Cahn–Hilliard-Type Equations with Logarithmic Potential. *SIAM Journal on Mathematical Analysis*, 52(5):5155–5195, 2020.

[48] Peter W Bates and Jianlong Han. The Neumann boundary problem for a nonlocal Cahn–Hilliard equation. *Journal of Differential Equations*, 212(2):235–277, 2005.

[49] Florentina Tone and Djoko Wirosoetisno. On the long-time stability of the implicit euler scheme for the two-dimensional Navier–Stokes equations. *SIAM journal on Numerical Analysis*, 44(1):29–40, 2006.

[50] Sean Breckling and Sidney Shields. The long-time L^2 and H^1 stability of linearly extrapolated second-order time-stepping schemes for the 2D incompressible Navier–Stokes equations. *Applied Mathematics and Computation*, 342:263–279, 2019.

[51] Leo G.Rebholz and Florentina Tone. Long-time H^1-stability of BDF2 time stepping for 2D Navier–Stokes equations. *Applied Mathematics Letters*, 141:108624, 2023.

[52] Kelong Cheng and Cheng Wang. Long time stability of high order multistep numerical schemes for two-dimensional incompressible Navier–Stokes equations. *SIAM Journal on Numerical Analysis*, 54(5):3123–3144, 2016.

[53] Sigal Gottlieb, Florentina Tone, Cheng Wang, Xiaoming Wang, and Djoko Wirosoetisno. Long time stability of a classical efficient scheme for two-dimensional Navier–Stokes equations. *SIAM Journal on Numerical Analysis*, 50(1):126–150, 2012.

[54] Xiaoming Wang. An efficient second order in time scheme for approximating long time statistical properties of the two dimensional Navier–Stokes equations. *Numerische Mathematik*, 121(4):753–779, 2012.

[55] Florentina Tone. On the long-time H^2-stability of the implicit euler scheme for the 2D magnetohydrodynamics equations. *Journal of Scientific Computing*, 38:331–348, 2009.

[56] Jie Shen. Convergence of approximate attractors for a fully discrete system for reaction-diffusion equations. *Numerical functional analysis and optimization*, 10(11-12):1213–1234, 1989.

[57] Jie Shen. Long time stability and convergence for fully discrete nonlinear Galerkin methods. *Applicable Analysis*, 38(4):201–229, 1990.

[58] Morgan Pierre. Convergence of exponential attractors for a time semi-discrete reaction-diffusion equation. *Numerische Mathematik*, 139(1):121–153, 2018.

[59] Wansheng Wang, Zheng Wang, and Zhaoxiang Li. Long time H^s_α stability of a classical scheme for Cahn-Hilliard equation with polynomial nonlinearity. *Applied Numerical Mathematics*, 165:35–55, 2021.

[60] Wansheng Wang and Yi Huang. Analytical and numerical dissipativity for the space-fractional Allen–Cahn equation. *Mathematics and Computers in Simulation*, 207:80–96, 2023.

[61] Haim Brezis and Haim Brézis. *Functional analysis, Sobolev spaces and partial differential equations*. Springer, 2011.

[62] Louis Nirenberg. On elliptic partial differential equations. *Annali della Scuola Normale Superiore di Pisa-Scienze Fisiche e Matematiche*, 13(2):115–162, 1959.

[63] Louis Nirenberg. An extended interpolation inequality. *Annali della Scuola Normale Superiore di Pisa-Scienze Fisiche e Matematiche*, 20(4):733–737, 1966.

[64] Jie Shen and Xiaofeng Yang. Numerical approximations of Allen-Cahn and Cahn-Hilliard equations. *Discrete Contin. Dyn. Syst*, 28(4):1669–1691, 2010.

[65] Jing Guo, Cheng Wang, Steven M Wise, and Xingye Yue. An improved error analysis for a second-order numerical scheme for the Cahn–Hilliard equation. *Journal of Computational and Applied Mathematics*, 388:113300, 2021.

[66] Jing Guo, Cheng Wang, Steven M Wise, and Xingye Yue. An H^2 convergence of a second-order convex-splitting, finite difference scheme for the three-dimensional Cahn–Hilliard equation. *Communications in Mathematical Sciences*, 14(2):489–515, 2016.

[67] Xiao Li, Zhonghua Qiao, and Cheng Wang. Stabilization parameter analysis of a second-order linear numerical scheme for the nonlocal Cahn–Hilliard equation. *IMA Journal of Numerical Analysis*, 43(2):1089–1114, 2023.

[68] Xiao Li, Zhonghua Qiao, and Cheng Wang. Double stabilizations and convergence analysis of a second-order linear numerical scheme for the nonlocal Cahn-Hilliard equation. *Science China Mathematics*, 67(1):187–210, 2024.

[69] Roxana Alexandru and Pier Luigi Dragotti. Reconstructing classes of non-band limited signals from time encoded information. *IEEE Transactions on Signal Processing*, 68:747–763, 2019.

[70] Qiang Du, Yunzhe Tao, Xiaochuan Tian, and Jiang Yang. Robust a posteriori stress analysis for quadrature collocation approximations of nonlocal models via nonlocal gradients. *Computer Methods in Applied Mechanics and Engineering*, 310:605–627, 2016.

[71] Adam Chmaj and Xiaofeng Ren. Homoclinic solutions of an integral equation: existence and stability. *Journal of differential equations*, 155(1):17–43, 1999.

[72] Zhou Wang, Alan C Bovik, Hamid R Sheikh, and Eero P Simoncelli. Image quality assessment: from error visibility to structural similarity. *IEEE transactions on image processing*, 13(4):600–612, 2004.